A smoothly curved body skimming on shallow water

Kevin Liu and Frank T. Smith

UCL, Gower St, Bloomsbury, London WC1E 6BT, UK

Abstract

We investigate the dynamics of a smoothly curved convex body skimming on a layer of shallow water, with the phenomenon of skipping stones as a primary modelling motivation but also industrial applications in mind. The skimming process of such an object may consist of two successive stages: an impact stage and a conditional planing stage. The focus here is on explaining the change from one stage to the other, with the body movement responding freely to the fluid flow pressures and vice-versa. We first introduce a water impact model and analyse the conditions under which a smooth body may rapidly transit to a planing motion via small time asymptotics. A planing model is then introduced, and in particular we investigate the effects of pressure conditions in the separation flow; we demonstrate under certain weak adverse pressure gradient conditions a smooth body's planing motion at early times can be seen as undergoing three successive transitory phases.

Keywords: Skimming, impact, planing, smooth body, shallow water.

1. Introduction

In this paper we study the dynamics of a smooth object skimming (skipping) on a layer of shallow water in two spatial dimensions. The motivation comes from modelling skipping stones, with wider applications to seaplane landing on relatively shallow water, ice crystals in cirrus clouds impacting on damp aircraft fuselage, jet-ski and speedboat safety, as well as other recreational activities such as surf skimming [18, 6, 7, 17, 22].

The topic of skimming, particularly by a thin body with sharp trailing edge (our model below has no sharp edge) on water with finite depth, has been subject to numerous investigations [2, 3, 5, 19, 13, 21]. In such cases water is assumed to detach smoothly from the body's sharp trailing edge, while ahead of the body water can be seen to "pile up" and a splash jet may

also be emitted [11]; one key modelling challenge of this problem is in determining the contact region between the body and fluid, whence obtaining the resulting lift force on the body. By contrast, in the case of a completely smooth body the added complexities are that the trailing separation position (the detachment point) acts as one additional unknown moving boundary, since there is no fixed sharp edge.

In general for the present smoothly curved body the skimming process can be decomposed into two successive stages [23, 26, 13] – an initial impact stage followed by a planing stage, after which the body either sinks or lifts off from water and thereby completes one skipping cycle. Rationally describing the transition from the impact stage to the planing stage is a challenge here. The specific aim of our paper here is two-fold: firstly we present a rapid impact and planing model, through which we analyse the conditions that enable a smooth body to rapidly transit from its initial impact to the planing stage; secondly we investigate the presence of adverse pressure gradient near the body's trailing separation point and its effect on the body's overall planing motion.

The early mathematical treatments of a solid object slamming on an undisturbed free surface of water were pioneered in [8, 9, 25]. See also [10, 20, 15, 12, 1, 22, 26]. The range of phenomena present can be complex and there are many parameters potentially involved. We focus on impact and planing through an analytical study. Our asymptotic analysis shows that during early touchdown the pressure underneath a smooth body is high everywhere, however as time progresses a sub-atmospheric pressure region begins to grow in its trailing separation region, which likely gives rise to separation and/or instability. Excellent work by [26] specifically investigated the phenomenon of a smooth body skimming on shallow water. Their analysis indicates that if we demand smooth flow separation by applying a Brillouin-Villat pressure condition as the body begins its planing motion, a discontinuity is predicted in the trailing separation position (compared with its position at the end of the impact stage). This is further analysed in [16] by examining three separation criteria in the trailing flow: the Brillouin-Villat condition, minimisation of change of fluid kinetic energy, and setting the separation point to be where the body-surface tangent is parallel to its body velocity; in all three cases discontinuities in the trailing separation position solutions are produced. We discuss the pressure conditions that give rise to such separation later. It is noted in passing that most works impose a prescribed body velocity whereas the present work allows free movement of the body.

Our paper is structured as follows. Section 2 presents the analysis of a smooth body impacting on a shallow layer of water; small time asymptotics

are then performed to investigate the conditions under which it is able to transit to a planing motion. We present the planing analysis in Section 3 and investigate conditions that may lead to modelled turbulent trailing flow separations. Such findings enable us to show in Section 4 that in a weak adverse pressure gradient regime a smooth body's planing motion can itself be viewed as three distinct and transitory phases. Section 5 provides conclusions.

2. Impact stage model development

The skimming object has an elongated horizontal profile whose length $\bar{l}$ is significantly greater than its thickness; its lower body surface which may be in contact with water is smooth and strictly convex. Let $\bar{h}$ be the depth of the water; it being shallow implies $\bar{h} \sim \epsilon\bar{l}$ with $\epsilon \ll 1$. This object skims at an inclined angle, say α with angular velocity ω, the angle of inclination being defined as the one made by the major axis and the undisturbed water surface and being small of order ϵ. Letting $(\bar{u}, \bar{v})$ be the body's horizontal and vertical velocity respectively, the horizontal component is a magnitude larger than the vertical, specifically $\bar{v} \sim \epsilon\bar{u}$. The flow is idealised to be incompressible and irrotational.

In a Cartesian coordinate system $(\bar{x}, \bar{y})$ as in Figure 1, the $\bar{y}$-axis passes through the skimming body's centre of mass, whose coordinate is $(0, \bar{y}_m)$ say. The coordinate system travels horizontally with the skimming body, the undisturbed water flows in the positive direction of the $\bar{x}$-axis and the body itself has only vertical and angular motions. To leading order the horizontal motion of the body remains at a uniform velocity because horizontal forces are relatively small.

As the body impacts on the water, the flow can be approximately divided into three sub-regions: an undisturbed up-stream flow region at rest relative to the ground (thus at uniform velocity approaching the body); a region near the leading contact position with elevated free surface of size $O(\bar{h}) \times O(\bar{h})$, known as the "jet-root" or "turn-over" region where the flow separates from the body and splash jets may be emitted; and a main flow region trapped under the body and enclosed by the jet-root regions. The splash jets are typically thin compared with the main body flow and their effects can be neglected [9, 5]. We let $\bar{x}_1$, $\bar{x}_2$ be the unknown horizontal positions of the stream turn-over points in the jet-root regions.

The typical Reynolds number is large in practice, as are the Froude and Weber numbers, and the flow is broadly pressure driven. That suggests nominally the Navier-Stokes equations can be approximated by the Euler

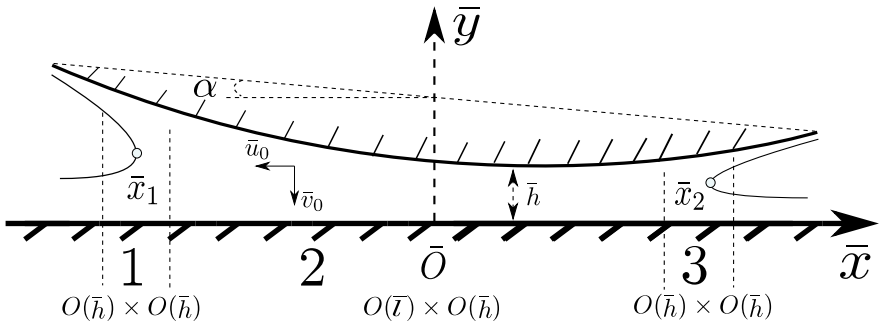

Figure 1: A close-up sketch of a smooth body during the impact stage of a skimming process. $\bar{x}_1$ and $\bar{x}_2$ represent the horizontal positions of the leading and trailing contact points respectively. $\bar{h}$ denotes the representative depth of the water layer, the jet root regions 1 and 3 have representative scales of $O(\bar{h}) \times O(\bar{h})$, while the region underneath the impact body has size of $O(\bar{l}) \times O(\bar{h})$. At a sufficiently small time, the contact surface of the smooth body can be approximated by a parabola at the leading order, and $\bar{x}_1$, $\bar{x}_2$ move away from each other at an extremely large speed.

form. Our non-dimensionalization is then based on the body length $\bar{l}$ and horizontal velocity $\bar{u}_0$: $x = \frac{\bar{x}}{\bar{l}}$, $y = \frac{\bar{y}}{\bar{l}}$, $h = \frac{\bar{h}}{\bar{l}}$, $u = \frac{\bar{u}}{\bar{u}_0}$, $v = \frac{\bar{v}}{\bar{u}_0}$, $t = \frac{\bar{l}}{\bar{u}_0}$, $p = \frac{\bar{p}}{\rho \bar{u}_0^2}$, $m = \frac{\bar{m}}{\rho \bar{l}^2}$, $i = \frac{\bar{i}}{\rho \bar{l}^4}$; $\bar{m}$ and $\bar{i}$ are the skipping stone's body mass and moment of inertia respectively.

Supposing the body's lower surface is given by $\eta(x)$, then the water depth under the body is simply: $h(x, \alpha, t) = y_m(t) + x\alpha(t) - \eta(x)$. Given its lower surface is smooth and convex, we stipulate that such surface can be written in a parabolic form: $\eta(x) = ax^2 + bx + c$. The coefficients a, b and c are constants and can be calibrated according to the object's body shape, with a being strictly negative due to our configuration. To ensure the skimming body has a large aspect ratio, the surface coefficients should be small, i.e. $a, b, c = O(\epsilon)$. The large differences between the horizontal and vertical scales can be further exploited by introducing the following scaling:

$$(\alpha, \eta, y, h, a, b, c) = \epsilon \times (\theta, T, Y, H, A, B, C), \tag{1}$$

where $\epsilon = \bar{h}_0/\bar{l} \ll 1$ as before. Hence the equations of the water depth and the body surface can be written conveniently as:

$$H(x, \theta, t) = Y_m(t) + x\theta(t) - T(x), \qquad T(x) = Ax^2 + Bx + C, \tag{2}$$

where $A < 0$. Supposing the initial point of impact is (x_0, H_0) we readily obtain $x_0 = \frac{\theta_0 - B}{2A}$, with θ_0 being the initial contact angle at touchdown. As one would expect the initial contact location is dependent upon the skimming body's contact angle and its surface geometry.

Since the flow is irrotational the kinematic boundary condition at the surface of the flow can be written as:

$$\frac{\partial H}{\partial t} + \frac{\partial (uH)}{\partial x} = 0; \tag{3}$$

similarly the horizontal momentum balance reduces to

$$\frac{\partial u}{\partial t} + u\frac{\partial u}{\partial x} = -\frac{\partial p}{\partial x}. \tag{4}$$

As the model flow is predominantly pressure driven, we have the following vertical and angular momentum equations for the body:

$$M\frac{d^2 Y_m}{dt^2} = \int_{x_1}^{x_2} p(x,t)dx \tag{5a}$$

$$I\frac{d^2\theta}{dt^2} = \int_{x_1}^{x_2} xp(x,t)dx, \tag{5b}$$

where $(M, I) = \epsilon(m, i)$.

Concerning boundary conditions, during the impact phase the speeds at which the leading- and trailing-separation positions travel away from the initial touchdown point are extremely large, with spray jets formed from these edges. As jets are thrown into their respective up and down streams, part of the fluid momentum is lost; under the assumptions of inviscid flow this loss of momentum is balanced by the force caused by the pressure difference between that of the jet root regions and the atmosphere, giving the pressure jump condition used by [5, 19, 26]. This pressure jump condition and Bernoulli's principle serve as boundary conditions to our impact problem (here $n = 1, 2$):

$$p(x_n,t) + \frac{1}{2}\left(u(x_n,t) - \frac{dx_n}{dt}\right)^2 = \frac{1}{2}\left(1 - \frac{dx_n}{dt}\right)^2, \tag{6a}$$

$$\left(u(x_n,t) - \frac{dx_n}{dt}\right) \Big/ \left(1 - \frac{dx_n}{dt}\right) = 2H(x_n,t)^{-\frac{1}{2}} - 1. \tag{6b}$$

The current impact model therefore consists of (2) - (6). The solution to this integro-differential system is challenging as the contact surface (x_1, x_2)

needs to be determined as part of the solution. Full numerical treatments have been studied by [4, 26], whereas we focus on a short-time formulation for further analytical insights.

2.1. Rapid impact model development

During the impact phase the solid-liquid contact surface initially goes through a phase of rapid expansion and spray jets are formed at the boundary of the surface. As time progresses if the skimming body is able to transit from impact to planing phase, such a transition is marked by the disappearance of the spray jet from the trailing separation point.

Our analysis here focuses on short times after impact when t $(= \delta\hat{t})$ is of order δ where $\delta \ll 1$. On this time scale the free surface penetration is small and of order t; balancing the terms of the free surface equation (2) suggests the model's horizontal and angular scales both evolve at order of $t^{\frac{1}{2}}$, which is consistent with Wagner's theory of vertical impacts by a body with a parabolic shape of course (see [24, 20]); the boundary conditions indicate the fluid's horizontal velocity u evolves on the same scale as x, i.e. order $t^{\frac{1}{2}}$, while the pressure p on the other hand is inferred to be of order unity. We therefore asymptotically expand the system variables as follows:

$$\begin{aligned} &t = \delta\hat{t},\ \ x \sim x_0 + \delta^{\frac{1}{2}}\hat{x} + O(\delta),\ \ \theta \sim \theta_0 + \delta^{\frac{1}{2}}\hat{\theta} + O(\delta),\ \ p \sim \hat{p} + O(\delta^{\frac{1}{2}}) \\ &Y_m \sim Y_0 + \delta\hat{Y} + O(\delta^2),\ \ H \sim 1 + \delta\hat{H} + O(\delta^2),\ \ u \sim 1 + \delta^{\frac{1}{2}}\hat{u} + O(\delta). \end{aligned} \tag{7}$$

The contact surface elevation equation (2) immediately yields $x_0 = 0$, $\theta_0 = B$, $Y_0 = T(x_0)$, $\hat{H} = \hat{Y} + \hat{x}\hat{\theta} - A\hat{x}^2$. Based on the asymptotics of (7) our impact model (2) - (6) simplifies to a pair of differential-algebraic equations (DAEs):

$$2A(\hat{x}_1^2 + \hat{x}_1\hat{x}_2 + \hat{x}_2^2) - 3\hat{\omega}_0\hat{t}(\hat{x}_1 + \hat{x}_2) - 6\hat{V}_0\hat{t} = 0, \tag{8a}$$

$$6\big[A\hat{x}_1^2 - \hat{\omega}_0\hat{t}\hat{x}_1 - \hat{V}_0\hat{t}\big]\frac{d\hat{x}_1}{d\hat{t}} + 6\big[A\hat{x}_2^2 - \hat{\omega}_0\hat{t}\hat{x}_2 - \hat{V}_0\hat{t}\big]\frac{d\hat{x}_2}{d\hat{t}} - \hat{\omega}_0(\hat{x}_1 - \hat{x}_2)^2 = 0, \tag{8b}$$

where $\hat{x}_1$, $\hat{x}_2$, i.e. the horizontal positions of the leading and trailing flow separation points respectively, are unknowns.

For small times $\hat{t}$ the system gives:

$$\hat{x}_1 \sim \frac{\hat{\omega}_0 + \big(192AV_0 - 3\hat{\omega}_0^2\big)^{\frac{1}{2}}}{8A}\hat{t}^{\frac{1}{2}}, \quad \hat{x}_2 \sim \frac{\hat{\omega}_0 - \big(192AV_0 - 3\hat{\omega}_0^2\big)^{\frac{1}{2}}}{8A}\hat{t}^{\frac{1}{2}}. \tag{9}$$

Thus we see immediately that for a skimming body with no angular rotation ($\hat{\omega}_0 = 0$), its leading and trailing points evolve away from the initial touch-down point at constant and equal speeds of order $\hat{t}^{-\frac{1}{2}}$. A positive rotation of the body where $\hat{\omega}_0 > 0$, i.e. the body that "rotates forwards", would result in the leading point extending away from the touch down point at a faster pace than the trailing point, and vice-versa for a body with negative rotation, which intuitively makes physical sense. The speed at which the two separation points evolve has an inverse relation with the skimming body's curvature: if the curvature coefficient is small, i.e. $A \ll 1$, the body becomes very similar to that of a flat plate and the speed at which the two points travel away from each other becomes very large. Notice that for a body with positive rotation $\hat{\omega}_0 > 0$, (9) indicate the trailing separation point's speed decreases more rapidly when compared with that of the leading one, and asymptotically approaches zero as time increases.

At large time $\hat{t}$ on the other hand, we can expect the two separation points to evolve on the same order as the body's vertical scale [14]. The asymptotes are found to be linear in $\hat{t}$, suggesting that there are no retractions of either separation positions in the early impact time regime for a skimming body with order unity body mass.

2.2. Rapid transition to planing stage

The analysis from the previous section shows that for a short time after impact, the hydrodynamic pressure underneath the skimming body does not generate sufficient lift to alter its vertical trajectory at the leading order, and the wetted edges extend away from the initial contact point on a square-root time scale as in (9). It is possible however, for the body to go through a rapid transition from impact to the subsequent planing phase. For a body whose mass is sufficiently small ($O(\delta^{\frac{3}{2}})$), its vertical momentum equation becomes non-trivial to the leading order and its motion can no longer be approximated by the initial impact velocity; instead the body feels the effect of the hydrodynamic pressure force very soon indeed after impact:

$$M\frac{d^2\hat{Y}}{d\hat{t}^2} = \int_{\hat{x}_1}^{\hat{x}_2} \hat{p}d\hat{x}. \tag{10}$$

We note that a rotating body's moment of inertia $\bar{i}$ has an upper bound of $\bar{m}\bar{l}^2$, or in our non-dimensionalised regime: $I \leq M$. This would indicate at face value that its angular momentum must also be proportionately scaled. In the physical world however, a skipping stone can be given a spin to help stabilise its contact angle with water; in three dimensions this would be

about a z-axis perpendicular to our two- dimensional plane. Such angle stabilisation via the gyroscopic effect cannot be captured "as it is" in our model, but rather approximated by having a relatively large moment of inertia. In theory if the body has a very large spin about its z-axis such that it maintains a steady contact angle from touchdown to an eventual exit, this can be captured in our model by having a moment of inertia that is an order of magnitude greater than the mass: $I \gg M$. Moreover, even if I is of the same order $\delta^{\frac{3}{2}}$ as M, the angular motion of the body still gives us the same relation as that holding for $I \gg M$, namely $\theta_{tt} = 0$: in fact the relation continues to apply for all I greater than $\delta^{\frac{5}{2}}$. This property adds weight to the argument favouring (10) as the main new feature.

These steps are found to lead our impact model to take on the following small time asymptotic form:

$$\hat{Y} = \frac{1}{3}A(\hat{x}_1^2 + \hat{x}_1\hat{x}_2 + \hat{x}_2^2) - \frac{1}{2}\hat{\omega}_0(\hat{x}_1 + \hat{x}_2)\hat{t}, \tag{11a}$$

$$\hat{f} = -\frac{1}{6}\hat{\omega}_0(\hat{x}_1^2 + \hat{x}_1\hat{x}_2 + \hat{x}_2^2) - \frac{1}{2}(\hat{x}_1 + \hat{x}_2)\frac{d\hat{Y}}{d\hat{t}}, \tag{11b}$$

$$\hat{f} = \frac{1}{2}\frac{d}{d\hat{t}}\left[\frac{A}{3}(\hat{x}_1^3 + \hat{x}_2^3) - \frac{\hat{\omega}_0}{2}(\hat{x}_1^2 + \hat{x}_2^2)\hat{t} - (\hat{x}_1 + \hat{x}_2)\hat{Y}\right], \tag{11c}$$

$$\hat{g} = -\frac{1}{2}\frac{d}{d\hat{t}}\left[\frac{\hat{\omega}_0}{6}(\hat{x}_1^3 + \hat{x}_2^3) + \frac{1}{2}(\hat{x}_1^2 + \hat{x}_2^2)\frac{d\hat{Y}}{d\hat{t}} + (\hat{x}_1 + \hat{x}_2)\hat{f}\right], \tag{11d}$$

$$(6M + \hat{x}_1^3 - \hat{x}_2^3)\frac{d^2\hat{Y}}{d\hat{t}^2} + 3(\hat{x}_1^2 - \hat{x}_2^2)\frac{d\hat{f}}{d\hat{t}} + 6(\hat{x}_1 - \hat{x}_2)\hat{g} = 0. \tag{11e}$$

The system consists of five DAEs with five unknowns $\hat{x}_1$, $\hat{x}_2$, $\hat{Y}$, $\hat{f}$ and $\hat{g}$. Numerical results are shown in Fig. 2 for a body with positive angular rotation $\hat{\omega}_0 > 0$.

The results indicate a retraction of either the leading or trailing contact point. At touchdown the speed at which the leading and trailing points evolve away from the initial point of impact is large. This rapid expansion of contact area slows down as time progresses, and the trailing point's velocity eventually drops to zero as demonstrated in Fig. 2b. Letting $\hat{t}_c$ denote the critical time when this phenomenon occurs, $\hat{t}_c$ is estimated to be 1.0497 with the initial conditions of $\hat{\omega}_0 = 1$ and $\hat{V}_0 = -1$. Before then we see in Fig. 2c that the fluid velocity at the leading point is negative as expected, i.e. fluid flows away from the skimming body towards upstream. At the trailing point the fluid velocity is positive but as the critical time $\hat{t}_c$ is approached it gradually decreases to zero. This also corresponds to the trailing point's

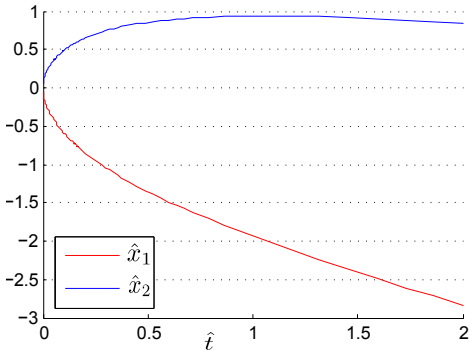

(a) Evolution of leading and trailing separation positions $\hat{x}_1$, $\hat{x}_2$ w.r.t. time $\hat{t}$.

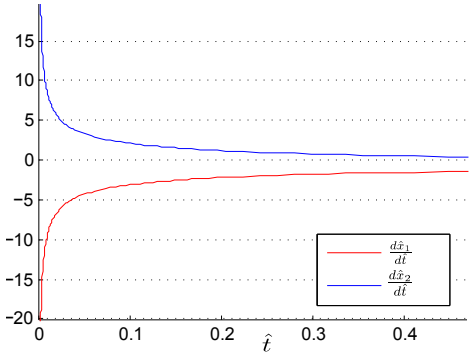

(b) Evolution of leading and trailing separation positions' velocities $\frac{d\hat{x}_1}{d\hat{t}}$, $\frac{d\hat{x}_2}{d\hat{t}}$.

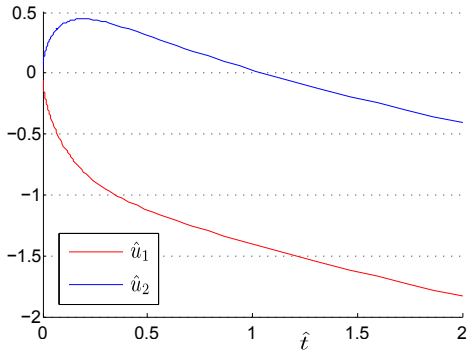

(c) The evolution of fluid velocities $\hat{u}_1$ and $\hat{u}_2$.

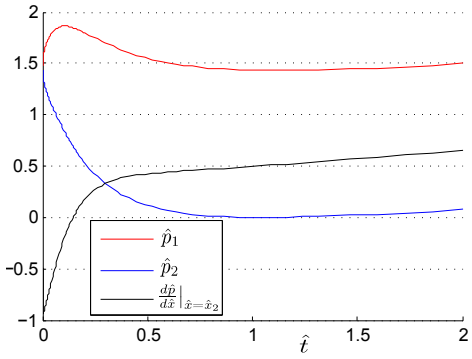

(d) Evolution of leading and trailing separation pressure profiles.

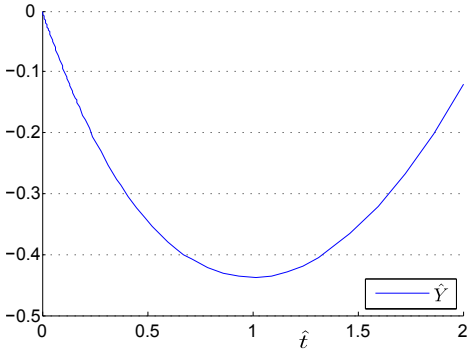

(e) Vertical evolution of the skimming body's centre of mass.

Figure 2: Profile plots of a skimming body with a positive rotation $\hat{\omega}_0 > 0$. The initial vertical velocity of the body $\hat{V}_0$ is taken to be -1, and the initial angular velocity $\hat{\omega}_0$ is taken to be 1. Under these initial settings the trailing separation point $\hat{x}_2$ initially evolves towards the downstream, however at time $\hat{t} \approx 1.0497$ this separation point reaches its maximum and begins to retract towards upstream.

pressure $\hat{p}_2$ dropping to zero / atmospheric as dictated by our pressure jump conditions and illustrated in Fig. 2d. The vertical centre of mass position $\hat{Y}$ reaches its minimum at $\hat{t} \approx 0.9887$ shortly before the critical time $\hat{t}_c$, and starts to move upwards and thus is in the early stages of heading towards exiting the water just before the trailing point's pressure drops to zero at $\hat{t} = \hat{t}_c$. In the case of a negative angular rotation, the same behaviour is true except that it occurs at the leading separation point. This suggests that the angular velocity of the body has an important and immediate effect after impact, influencing the evolution of the wetted contact area and thus the pressure lift force. Once the critical time is reached a planing model is needed subsequently to describe the next stage of the skimming process for times $\hat{t}$ beyond $\hat{t}_c$.

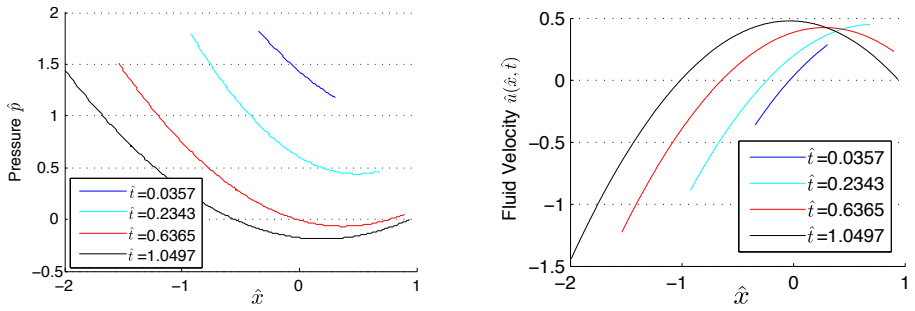

(a) A plot of pressure profiles $\hat{p}$ underneath the skimming body at different times of the impact stage.

(b) A plot of fluid velocity profiles $\hat{u}$ underneath the skimming body at different times of the impact stage.

Figure 3: The time evolution of the pressure and fluid velocity underneath the skimming body during the impact stage for a positively rotating body. The time begins from shortly after impact $\hat{t} = 0.0357$ to the end of impact stage at $\hat{t} = 1.0497$ when the trailing separation pressure drops to zero. Notice that the wetted surface area is initially small and increases over time. The initial conditions are $\hat{V}_0 = -1$ and $\hat{\omega}_0 = 1$.

Fig. 3a shows a snapshot of the hydrodynamic pressure under a positively rotating body over time. A short time after impact the pressure is high and positive everywhere as depicted at $\hat{t} = 0.0357$. As time progresses the wetted surface area grows, the pressure starts to decrease everywhere and eventually a negative pressure region develops near the trailing point as shown at $\hat{t} = 0.6365$. We notice there is an adverse pressure gradient field inside this negative pressure region [14]. The region expands over time and eventually reaches the trailing separation point, while the fluid velocity drops to zero as shown in Fig. 3b.

3. Planing stage

The transition from impact to planing stage is signified by the body's trailing point ceasing to extend downstream and the disappearance of the spray jet at this end. During planing as water from upstream comes in contact with the body, part of it is thrown back upstream from the leading separation point and the pressure jump conditions of (6a, 6b) still apply; the rest of the stream flows underneath the body and exits to downstream via a negative pressure gradient field in the trailing separation or detachment region.

Suppose for a moment that the flow can separate smoothly from the trailing detachment point with a laminar or turbulent boundary layer, where there is no presence of adverse pressure gradient of the sort we witnessed at the end of the impact stage, i.e. imposing the Brillouin-Villat (B.V.) pressure condition at this end by: $p(x_2, t) = \frac{\partial p}{\partial x}\big|_{x=x_2} = 0$. An immediate knock-on effect of this assumption is that a discontinuity in the solution of the trailing separation position arises when the body transitions from impact to planing motion, as indicated by [16, 26]. Under the B.V. condition, the trailing separation position is more upstream than that predicted by the pressure jump conditions at the end of the impact stage and so the demand of a perfectly smooth separation inevitably leads to a "jump" of the trailing detachment position during transition.

We can, on the other hand, impose a set of boundary conditions that allows the adverse pressure gradient to be carried over from the end of the impact stage [14]. Such an adverse pressure gradient leads to the boundary conditions:

$$p(x_2, t) = 0, \qquad \left.\frac{\partial p}{\partial x}\right|_{x=x_2} = \kappa, \tag{12}$$

where the B.V. conditions can be viewed as a special case with $\kappa = 0$.

The governing equations for the fluid flow and the planing body then are very similar to those of the impact model of (2) - (6), the difference being that: 1) in our planing model the time t starts at t^*, with t^* denoting the time at the end of the impact stage; and 2) at the unknown moving trailing point the momentum and pressure jump conditions (6a, 6b) are replaced by the separation conditions of (12), with the unknowns being Y_m, θ, u, p and with κ being a free parameter subject to user prescription, provided that $\kappa \geq 0$, i.e. maintaining an adverse pressure gradient at the trailing separation point.

In the sections that follow we continue from the impact stage analysis of Section 2.2 and investigate the planing behaviour via small time asymptotics.

3.1. Rapid planing model

Under the asymptotic regime of (7) we have the following reduced planing model:

$$\begin{aligned} &\frac{\partial \hat{H}}{\partial \hat{t}} + \frac{\partial \hat{u}}{\partial \hat{x}} = 0, \quad \frac{\partial \hat{p}}{\partial \hat{x}} + \frac{\partial \hat{u}}{\partial \hat{t}} = 0, \quad \hat{H} = \hat{Y} + \hat{x}\hat{\theta} - A\hat{x}^2, \\ &M\frac{d^2\hat{Y}}{d\hat{t}^2} = \int_{\hat{x}_1}^{\hat{x}_2} \hat{p} d\hat{x}, \quad \frac{d^2\hat{\theta}}{d\hat{t}^2} = 0, \end{aligned} \tag{13}$$

with the boundary conditions at the leading and trailing positions as:

$$\begin{aligned} &\hat{p}(\hat{x}_1, \hat{t}) = \frac{d\hat{x}_1}{d\hat{t}}\hat{u}(\hat{x}_1, \hat{t}), \quad \hat{u}(\hat{x}_1, \hat{t}) = \frac{d\hat{x}_1}{d\hat{t}}\hat{H}(\hat{x}_1, \hat{t}), \\ &\hat{p}(\hat{x}_2, \hat{t}) = 0, \qquad\qquad \left.\frac{\partial \hat{p}}{\partial \hat{x}}\right|_{\hat{x}=\hat{x}_2} = \hat{\kappa}. \end{aligned} \tag{14}$$

Here $\hat{\kappa}$ denotes $\delta^{\frac{1}{2}}\kappa$. This planing-model system can be simplified by taking advantage of the fact that $\hat{\theta} = \hat{\omega}_0\hat{t}$ where $\hat{\omega}_0 > 0$ to obtain:

$$\left[6M + (\hat{x}_1 - \hat{x}_2)^3\right]\frac{d^2\hat{Y}}{d\hat{t}^2} + 3\hat{\kappa}(\hat{x}_1 - \hat{x}_2)^2 = 0, \tag{15a}$$

$$\frac{1}{2}(\hat{x}_1 - \hat{x}_2)^2\frac{d^2\hat{Y}}{d\hat{t}^2} + (A\hat{x}_1^2 - \hat{\omega}_0\hat{t}\hat{x}_1 - \hat{Y})\left(\frac{d\hat{x}_1}{d\hat{t}}\right)^2 + \hat{\kappa}(\hat{x}_1 - \hat{x}_2) = 0, \tag{15b}$$

$$\begin{aligned} &(\hat{x}_1 - \hat{x}_2)\frac{d^2\hat{Y}}{d\hat{t}^2} - (A\hat{x}_1^2 - \hat{\omega}_0\hat{t}\hat{x}_1 - \hat{Y})\frac{d^2\hat{x}_1}{d\hat{t}^2} - (2A\hat{x}_1 - \hat{\omega}_0\hat{t})\left(\frac{d\hat{x}_1}{d\hat{t}}\right)^2 \\ &\quad + 2\left(\hat{\omega}_0\hat{x}_1 + \frac{d\hat{Y}}{d\hat{t}}\right)\frac{d\hat{x}_1}{d\hat{t}} + \hat{\kappa} = 0. \end{aligned} \tag{15c}$$

Although the pressure gradient $\hat{\kappa}$ is a parameter whose value needs to be prescribed subject to physical constraints, we nevertheless have a few observations on its range: firstly, it has a lower bound of zero which is equivalent to the B.V. separation conditions as aforementioned; secondly, as we shall demonstrate, the more severe this adverse pressure gradient is, the further the flow remains attached to the under-surface of the planing body; finally, there is an upper limit on the severity of the adverse pressure gradient before our model's planing motion breaks down. While this limit is difficult

to obtain explicitly as it inherently depends on the dynamics carried over from the impact regime, we can derive a few implications of this limit on the body's planing behaviour.

3.2. Planing model solutions

Fig. 4 shows the numerical solutions of the planing system (15) for varying values of $\hat{\kappa}$ in the range between zero and 0.5076, the latter of which is the pressure gradient estimated from the end of the impact stage for $M = 1$ and $\hat{\omega}_0 = 1$. Notice the solution for the trailing separation position is only discontinuous for $\hat{\kappa} = 0$ when switching from the impact to the planing model. For small values of $\hat{\kappa}$ as illustrated in the case of $\hat{\kappa} = 0.1$, $\hat{x}_2$ converges to $\hat{x}_1 + (6M)^{\frac{1}{3}}$ over time, which is the solution under the B.V. condition as can be seen by setting $\hat{\kappa} = 0$ in equation (15a). If on the other hand the pressure gradient is higher than that observed at the end of the impact stage, specifically $\hat{\kappa} > 0.5076$, the flow separation takes place further downstream and effectively enlarges the fluid-body contact surface. This can be seen in the evolution of the trailing point position $\hat{x}_2$ relative to $\hat{x}_1$ in Fig. 5 for time $\hat{t} <\sim 1.6$.

Fig. 6 demonstrates a bifurcation behaviour in the solutions of the trailing separation position over larger values of $\hat{\kappa}$: if this value exceeds a certain limit (see $\hat{\kappa} \geq 0.607$) the solution breaks down over time, whereas below the limit the detachment position eventually retracts physically sensibly towards upstream.

To see there is a maximum sustainable adverse pressure gradient, we can combine model equations (15a), (15b) by eliminating $\frac{d^2\hat{Y}}{d\hat{t}^2}$ to obtain:

$$\frac{1}{2}\hat{\xi}^4 + 6M\hat{\xi} = \hat{\alpha}(6M - \hat{\xi}^3), \tag{16}$$

where $\hat{\xi} = \hat{x}_2 - \hat{x}_1$, $\hat{\alpha} = \hat{\eta}/\hat{\kappa}$, $\hat{\eta} = (A\hat{x}_1^2 - \hat{\omega}_0\hat{t}\hat{x}_1 - \hat{Y})(\frac{d\hat{x}_1}{d\hat{t}})^2$; note that $\hat{\xi}$ is positive and $\hat{\eta}$, $\hat{\alpha}$ take on negative values. We denote the left and right hand sides of (16) as f_L and f_R, which are quartic and cubic functions of $\hat{\xi}$ respectively. Notice these two curves intersect only in the first quadrant of the $(\hat{\xi}, f)$ plane. There is a critical value $\hat{\alpha}_D$ such that these two curves share the same gradient at the point of intersection, while if $\hat{\alpha}$ exceeds the limit $\hat{\alpha}_D$ the two curves do not intersect. This critical value $\hat{\alpha}_D = \hat{\eta}_D/\hat{\kappa}_D$ gives rise to $\hat{\kappa}_D$, which is the maximum adverse pressure gradient that can be sustained at the trailing point; exceeding this limit the trailing point position becomes unreachable and our planing model breaks down. To find this single intersection point we combine equation (16) and its derivative

with respect to $\hat{\xi}$ to obtain: $\hat{\xi}_D^6 - 48M\hat{\xi}_D^3 - 72M^2 = 0$, for which we can immediately write down the solution of $\hat{\xi}_D$ as:

$$\hat{\xi}_D = [(24 + 18\sqrt{2})M]^{\frac{1}{3}}; \tag{17}$$

this corresponds to a maximum fluid-body contact region due to the adverse pressure gradient in the separation flow, which in our 2D model is denoted by the distance between $\hat{x}_1$ and $\hat{x}_2$. This limit is dependent on the body mass and intuitively the heavier the planing body, the wider apart the leading and trailing points are.

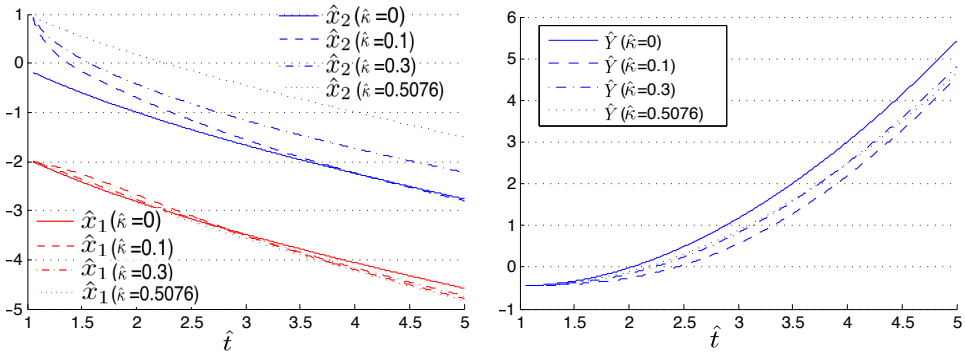

(a) The evolution of the body's leading and trailing detachment points during the planing stage.

(b) The evolution of the body's vertical centre of mass position during planing.

Figure 4: Plot of the leading and trailing detachment points, as well as the body's vertical centre of mass during the planing stage for varying values of $\hat{\kappa}$. The body's mass M and rotational velocity $\hat{\omega}_0$ are both taken to be one. For the case of $\hat{\kappa} = 0$ the trailing separation position $\hat{x}_2$ is not continuous when transitioning from impact to planing stage.

4. Small adverse pressure gradient at detachment point

The solutions in Fig. 4 indicate that for $\hat{\kappa}$ sufficiently small, the planing system converges in time to a state such that the leading and trailing separation points travel at a fixed distance of $(6M)^{\frac{1}{3}}$ from each other. The trailing one in particular goes through a phase of rapid adjustment in a short time span. We shall show that for a planing body subject to small adverse pressure gradient at the trailing separation region, i.e. $\hat{\kappa} \ll 1$, its planing motion can in effect be divided into three consecutive phases.

The first phase of the planing stage begins at the instant when the body completes its impact stage and enters the planing stage. The leading sep-

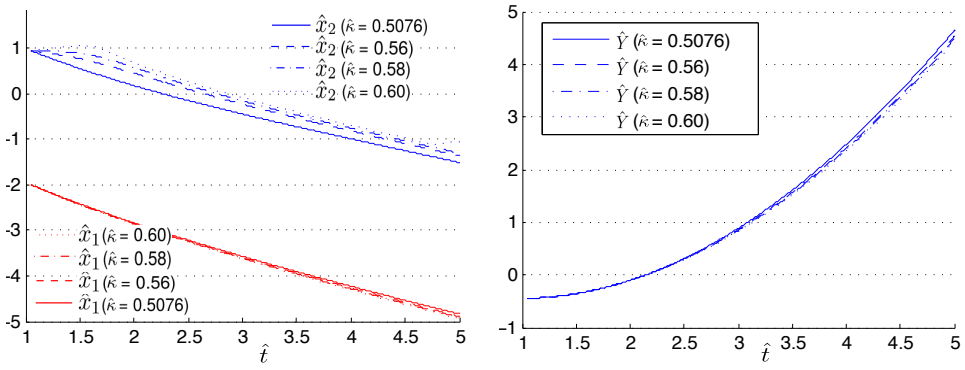

(a) The evolution of the body's leading and trailing points during the planing stage for varying values of $\hat{\kappa}$.

(b) The evolution of the body's vertical centre of mass position during planing for varying values of $\hat{\kappa}$.

Figure 5: Plot of the leading and trailing points, as well as the body's vertical centre of mass during the planing stage for varying values of trailing separation pressure gradient greater than that observed at the end of impact stage: $\hat{\kappa} > 0.5076$. We can observe that the trailing point position moves relatively further away from the leading point for $\hat{t} <\sim 1.6$. The body's mass M and rotational velocity $\hat{\omega}_0$ are both taken to be one.

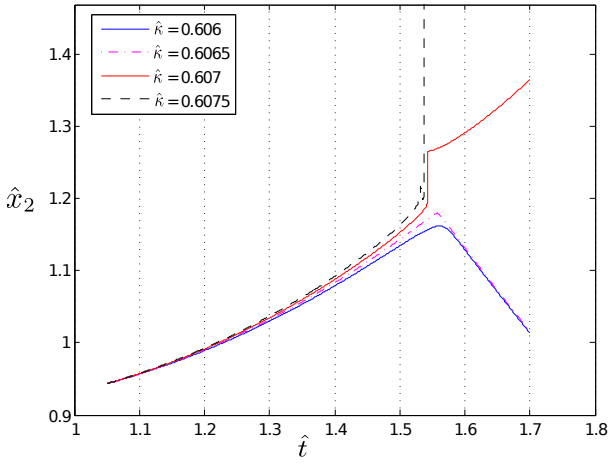

Figure 6: The unstable behaviour of trailing point position $\hat{x}_2$ for values of trailing separation pressure gradient $\hat{\kappa}$ exceeding an unknown upper limit.

aration point during this phase continues to move further upstream with its range on the scale of $\hat{\kappa}^{\frac{1}{2}}$, the trailing separation point in the meantime evolves in range scalable to order unity. At the end of the initial planing phase the distance between the two points becomes $(6M)^{\frac{1}{3}}$, in other words a planing system configured with a small trailing point adverse pressure gradient converges to that of the B.V. configuration. In the second planing stage the system evolves on a time scale of $\hat{\kappa}^{\frac{1}{4}}$, the evolution of the trailing point slows down from order unity to the same order as the leading point with a smaller adjustment ($O(\hat{\kappa}^{\frac{3}{4}})$). As time progresses the planing system eventually transitions to the final large time scale planing phase. During this phase the leading separation point evolves on a scale of order unity and the trailing point evolves in sync with its leading counterpart but with an $O(\hat{\kappa})$ adjustment.

4.1. Initial planing phase

This phase begins when the body transitions from impact to planing stage, supposing this time is $\hat{t}_c$ then we are concerned with $\hat{t} \geq \hat{t}_c$. Let $\hat{\xi} = \hat{x}_2 - \hat{x}_1$ as usual and let $\hat{x}_{c1}$, $\hat{Y}_c$ and $\hat{V}_c$ be the horizontal position of the leading separation point, vertical position of the centre of mass and vertical velocity respectively at this time. Assuming the trailing separation pressure gradient $\hat{\kappa}$ is small so that $0 < \hat{\kappa} \ll 1$, we can asymptotically expand the three system variables as:

$$\begin{aligned} &\hat{x}_1 = \hat{x}_{c1} + \hat{\kappa}^{\frac{1}{2}}\check{x}_1(\hat{t}) + O(\hat{\kappa}), \qquad \hat{\xi} = \check{\xi}_1(\hat{t}) + O(\hat{\kappa}^{\frac{1}{2}}), \\ &\hat{Y} = \hat{Y}_c + \hat{V}_c\hat{t} + \hat{\kappa}\check{Y}_1(\hat{t}) + O(\hat{\kappa}^2). \end{aligned} \tag{18}$$

Substituting into the planing system (15) yields the following relations at the leading order:

$$\frac{d}{d\hat{t}}\left[\zeta^2\frac{d\check{x}_1}{d\hat{t}}\right] = 0, \tag{19a}$$

$$\check{\xi}_1^4 + 2\zeta(6M - \check{\xi}_1^3)\left(\frac{d\check{x}_1}{d\hat{t}}\right)^2 + 12M\check{\xi}_1 = 0, \tag{19b}$$

$$[6M - \check{\xi}_1^3]\frac{d^2\check{Y}_1}{dt^2} + 3\check{\xi}_1^2 = 0, \tag{19c}$$

$$\zeta(\hat{t}) = \hat{x}_{c1}^2 + \hat{Y}_c + (\hat{V}_c + \hat{\omega}_0\hat{x}_{c1})\hat{t}, \tag{19d}$$

for which we need appropriate initial conditions for $\check{x}_1$, $\check{Y}_1$ at the beginning of the planing stage $\hat{t} = \hat{t}_c$, which we obtain as follows: let $\check{Y}_{10}$ and $\check{V}_{10}$ be the

initial value and first order derivative for $\check{Y}_1$ respectively; from the body's known vertical dynamics at this point we can deduce $\check{Y}_{10} \equiv \check{Y}_1(\hat{t}_c) = 0$, $\check{V}_{10} \equiv \frac{d\check{Y}_1}{d\hat{t}}(\hat{t}_c) = 0$; letting $\check{x}_{10}$ and $\check{u}_{10}$ be the initial value and first order derivative for $\check{x}_1$ respectively, then $\check{x}_{10}$ is zero by implication of (18) at time $\hat{t} = \hat{t}_c$, combining (19b, 19c) and setting $\hat{t} = \hat{t}_c$ produces the initial condition $\check{u}_{10} = -\left[\frac{\check{\xi}_{10}^4 + 12M\check{\xi}_{10}}{2\zeta_0(\check{\xi}_{10}^3 - 6M)}\right]^{\frac{1}{2}}$, where $\check{\xi}_{10} = \check{\xi}_1(\hat{t}_c)$, $\zeta_0 = \zeta(\hat{t}_c)$ and $\check{u}_{10} = \check{u}_1(\hat{t}_c)$ by the same notation convention.

These initial conditions yield the following solution for $\check{x}_1$:

$$\check{x}_1(\hat{t}) = \Phi_0(1 - \zeta_0\zeta^{-1}), \quad \Phi_0 = -\frac{\zeta_0}{\hat{V}_c + \hat{\omega}_0\hat{x}_{c1}}\left[\frac{\check{\xi}_{10}^4 + 12M\check{\xi}_{10}}{2\zeta_0(\check{\xi}_{10}^3 - 6M)}\right]^{\frac{1}{2}}. \quad (20)$$

This enables us to write down the following equation for $\check{\xi}_1$ from (19b):

$$\zeta^3\check{\xi}_1^4 - 2\Phi_0^2\check{\xi}_1^3 + 12M\zeta^3\check{\xi}_1 + 12M\Phi_0^2 = 0. \quad (21)$$

The formula for finding roots of quartic equations is well known and will not be presented here explicitly. Out of the four possible solutions for $\check{\xi}_1$ the admissible one should be real, positive and fit the physical context of the system. From (19c) we can obtain the solution for $\check{Y}_1$ in a double integral form based on the admissible solution of $\check{\xi}_1$:

$$\check{Y}_1 = \iint_{\hat{t}_c}^{\hat{t}} \frac{3\check{\xi}_1^2}{\check{\xi}_1^3 - 6M} d\hat{t}^2. \quad (22)$$

The solutions for $\check{x}_1$, $\check{\xi}_1$ and $\check{Y}_1$ are presented in Fig. 7. The results demonstrate that for a planing body with positive rotation, its leading separation position continues to extend in the direction of upstream as with the impact stage case. The trailing separation position on the other hand also begins to move in the direction of upstream, and it moves at a greater pace as demonstrated by the decreasing value of $\check{\xi}_1$ in Fig. 7b; this signifies the decrease of contact surface over time. During this phase the body continues to emerge from water as shown in Fig. 7c for the trajectory of its centre of mass.

4.2. Planing Phase II

The solution for $\check{x}_1$ depends inversely on $\zeta(\hat{t})$ given in (19d), whose value is positive at time $\hat{t}_c$ but decreases gradually, see Fig. 8. When ζ eventually reaches zero $\check{x}_1$ becomes singular and undefined. Supposing $\hat{t}_N$ is the time

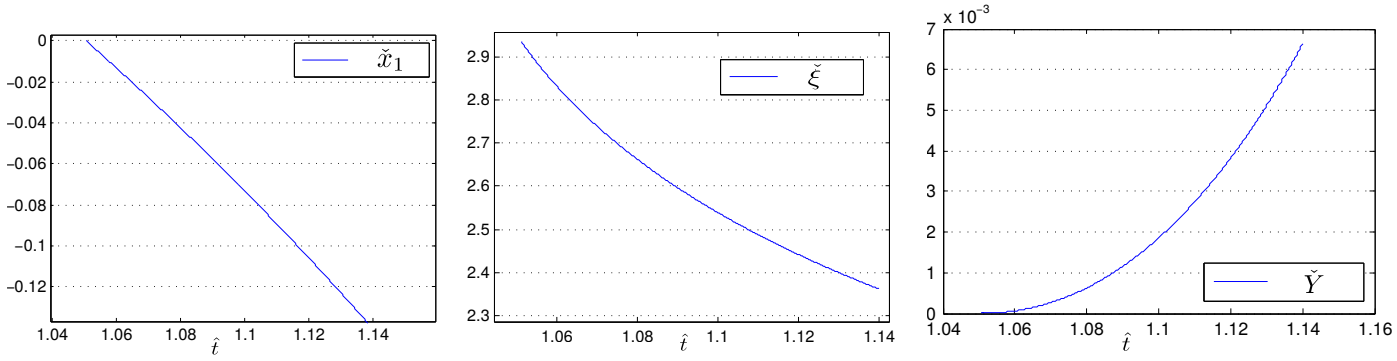

(a) $\check{x}_1$ (b) $\check{\xi}_1$ (c) $\check{Y}_1$.

Figure 7: Solutions of the planing system (19) with $M = 1$, $\hat{\omega}_0 = 1$, $\hat{\kappa} = 0.1$. The values of $\hat{x}_{c1}$, $\hat{x}_{c2}$, $\hat{Y}_c$ and $\hat{V}_c$ are the results from the final stage of impact model (11), their respective values are: -1.9944, 0.9434, -0.4431 and 0.0359.

when this singularity occurs then by (19d) we can immediately obtain

$$\hat{t}_N = -\frac{\hat{x}_{c1}^2 + \hat{Y}_c}{\hat{V}_c + \hat{\omega}_0 \hat{x}_{c1}}, \tag{23}$$

at which point $\check{\xi}_1$ takes on the value of $(6M)^{\frac{1}{3}}$ as can be seen by setting $\zeta(\hat{t}_N) = 0$ in (21). Thus at the end of phase I we arrive at the same solution as that given by the B.V. condition, and the time it takes to reach this solution is determined by the state of the system at the end of the impact stage as shown in (23). At the end of phase I the planing system no longer evolves on the scales described in (18) and a new evolution scale for the next planing phase is need.

The appropriate asymptotic scale for the next phase can be determined by inspecting the solution at times close to $\hat{t}_N$, namely $\hat{t} = \hat{t}_N + \delta_1 \bar{t}$ with $\delta_1 = \hat{\kappa}^{\frac{1}{4}}$, and in the second planing phase we thus have:

$$\begin{aligned} &\hat{t} = \hat{t}_N + \hat{\kappa}^{\frac{1}{4}} \bar{t}, && \hat{x}_1 = \hat{x}_{c1} + \hat{\kappa}^{\frac{1}{4}} \bar{x}_1, \\ &\hat{\xi} = (6M)^{\frac{1}{3}} - \hat{\kappa}^{\frac{3}{4}} \bar{\xi}_1, && \hat{Y}_1 = \hat{Y}_c + \hat{V}_c \hat{t}_N + \hat{\kappa}^{\frac{1}{4}} \hat{V}_c \bar{t} + \hat{\kappa}^{\frac{3}{4}} \bar{Y}_1. \end{aligned} \tag{24}$$

In essence the planing body's leading separation point and centre of mass move on a larger scale of $\hat{\kappa}^{\frac{1}{4}}$, while the trailing point moves on a scale comparable to its leading counterpart but with an $O(\hat{\kappa}^{\frac{3}{4}})$ adjustment. The

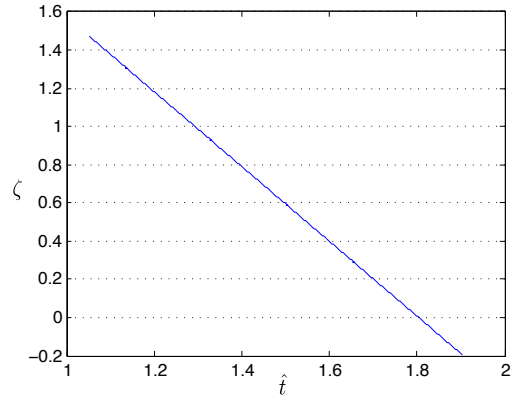

Figure 8: Solutions of $\zeta(\hat{t})$ during the planing phase. The values of $\hat{x}_{c1}$, $\hat{Y}_c$ and $\hat{V}_c$ are -1.9944, -0.4431 and 0.0359 respectively. $\zeta(\hat{t}_c)$ is positive; as time increases this eventually decreases to zero, at which point the solution for $\breve{x}_1$ becomes undefined.

planing model (15) now yields:

$$\begin{aligned}
&\bar{\xi}_1\ddot{\bar{Y}}_1 + 1 = 0, \quad \frac{1}{2}(6M)^{\frac{2}{3}}\ddot{\bar{Y}}_1 - \big[(2\hat{x}_{c1} + \hat{\omega}_0\hat{t}_N)\bar{x}_1 + (\hat{\omega}_0\hat{x}_{c1} + \hat{V}_c)\bar{t}\big]\dot{\bar{x}}_1^2 = 0, \\
&\big[(2\hat{x}_{c1} + \hat{\omega}_0\hat{t}_N)\bar{x}_1 + (\hat{\omega}_0\hat{x}_{c1} + \hat{V}_c)\bar{t}\big]\ddot{\bar{x}}_1 + (2\hat{x}_{c1} + \hat{\omega}_0\hat{t}_N)\dot{\bar{x}}_1^2 \\
&\qquad + 2(\hat{\omega}_0\hat{x}_{c1} + \hat{V}_c)\dot{\bar{x}}_1 = 0.
\end{aligned} \tag{25}$$

This system can be solved explicitly with initial conditions obtained by matching with phase I:

$$\bar{x}_1 = \frac{(C_1^2\bar{t}^2 - 2\Phi_0\zeta_0 C_2)^{\frac{1}{2}} - C_1\bar{t}}{C_2}, \tag{26a}$$

$$\bar{Y}_1 = \frac{2}{3}\frac{(C_1^2\bar{t}^2 - 2\Phi_0\zeta_0 C_2)^{\frac{3}{2}} - C_1^3\bar{t}^3}{(6M)^{\frac{2}{3}}C_2^2} + \frac{2\Phi_0\zeta_0 C_1\bar{t}}{(6M)^{\frac{2}{3}}C_2}, \tag{26b}$$

$$\bar{\xi}_1 = -\frac{(6M)^{\frac{2}{3}}C_2^2(C_1^2\bar{t}^2 - 2\Phi_0\zeta_0 C_2)^{\frac{1}{2}}}{2C_1^2\big[(C_1^2\bar{t}^2 - 2\Phi_0\zeta_0 C_2)^{\frac{1}{2}} - C_1\bar{t}\big]^2}, \tag{26c}$$

here $C_1 = \hat{\omega}_0\hat{x}_{c1} + \hat{V}_c$, $C_2 = 2\hat{x}_{c1} + \hat{\omega}_0\hat{t}_N$.

The solutions demonstrated in Fig. 9 indicate that the leading and trailing separation positions in this phase continue to move in the direction of upstream, and the pace at which the body emerges from the water significantly increases. As time progresses however our planing system will grow out of this $O(\hat{\kappa}^{\frac{1}{4}})$ scaling regime, which leads to the final and large time scale planing phase.

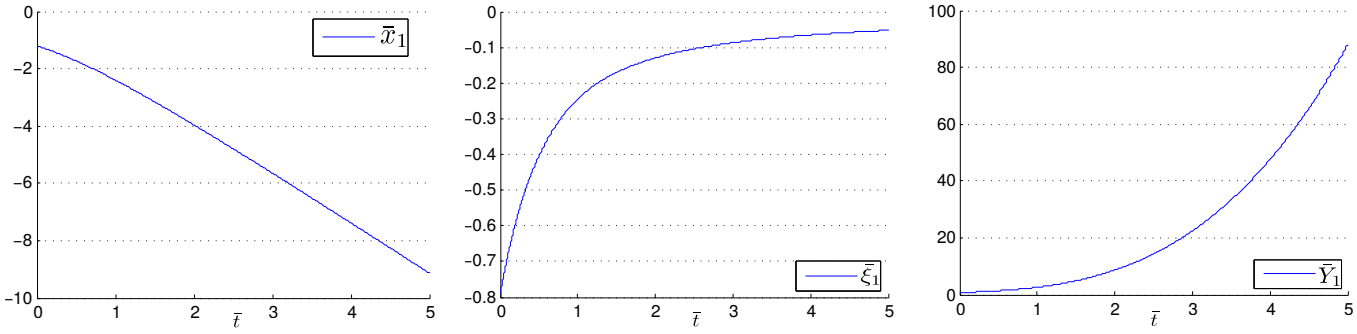

(a) $\bar{x}_1$ (b) $\bar{\xi}_1$ (c) $\bar{Y}_1$.

Figure 9: Plots of $\bar{x}_1$, $\bar{\xi}_1$ and $\bar{Y}_1$ over time $\bar{t} \in [0, 5]$. The values of $\hat{x}_{c1}$, $\hat{x}_{c2}$, $\hat{Y}_c$ and $\hat{V}_c$ are the results from the final stage of impact model (11), their respective values are: -1.9944, 0.9434, -0.4431 and 0.0359.

4.3. Planing Phase III

The appropriate scaling of this phase can be found by introducing a new time variable $\breve{t} = \hat{\kappa}^n \bar{t}$, where $0 < n < 1$ so that $\hat{\kappa}^n$ is small. Using a procedure similar to that in phase II it can be shown that $n = \frac{1}{4}$, and we are led to the following relations: $\hat{t} = \breve{t}$, $\hat{x}_1 = \breve{x}_1$, $\hat{\xi}_1 = (6M)^{\frac{1}{3}} - \hat{\kappa}\breve{\xi}_1$, $\hat{Y}_1 = \breve{Y}_1$, with the breve signs denoting the system variables for this final planing phase.

Substituting the above variable expansions into the the planing system of (15) gives the following planing system for phase III:

$$\begin{aligned} &\breve{\xi}_1 \ddot{\breve{Y}}_1 + 1 = 0, \quad \frac{1}{2}(6M)^{\frac{2}{3}} \ddot{\breve{Y}}_1 - (\breve{x}_1^2 + \hat{\omega}_0 \breve{t}\breve{x}_1 + \breve{Y}_1)(\dot{\breve{x}}_1)^2 = 0, \\ &(6M)^{\frac{1}{3}} \ddot{\breve{Y}}_1 - (\breve{x}_1^2 + \hat{\omega}_0 \breve{t}\breve{x}_1 + \breve{Y}_1)\ddot{\breve{x}}_1 - (2\breve{x}_1 + \hat{\omega}_0 \breve{t})(\dot{\breve{x}}_1)^2 \\ &\quad - 2(\hat{\omega}_0 \breve{x}_1 + \dot{\breve{Y}}_1)\dot{\breve{x}}_1 = 0. \end{aligned} \tag{27}$$

Explicit solutions to this coupled non-linear ODE system being difficult to obtain, numerical solutions are therefore pursued and the results are presented in Fig. 10. Comparisons with the solutions of the planing system (15) show this final planing phase system captures the body's behaviour at large times.

We see that during this phase the planing body continues to emerge from the water, and the leading and trailing detachment points continue to move upstream with their distance apart fixed at $(6M)^{\frac{1}{3}}$ to the leading order. The

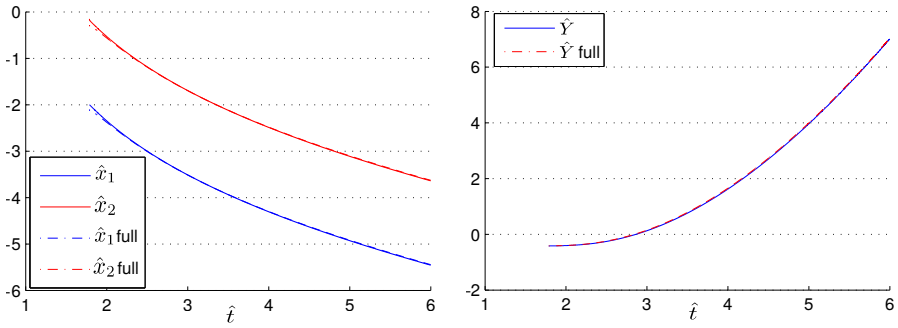

(a) Comparison of numerical solutions for $\hat{x}_1$, $\hat{x}_2$.

(b) Comparison of numerical solutions for $\hat{Y}$.

Figure 10: Numerical solutions of the planing system (27) compared with the full planing system (15) for $\hat{t} > \hat{t}_N$ and $\hat{\kappa} = 10^{-4}$.

large-time asymptotes are:

$$\breve{x}_1 = -\frac{1}{2}\hat{\omega}_0\breve{t}, \quad \breve{\xi} \to -\frac{2}{\hat{\omega}_0^2}, \quad \breve{Y} = \frac{1}{4}\hat{\omega}_0^2\breve{t}^2.$$

If we are able to see the planing body lifting off and separating from water, the positions of the leading and trailing points should eventually coincide as shown by [26] in numerical solutions of a planing system; this is not the case in our rapid planing model as the large time solutions demonstrate. Under the current planing regime, thus far, the body continues to lift upwards as time grows but the distance between the two wetted points does not decrease. As the body evolves vertically to the squared power of time it will eventually grow out of the rapid regime defined in (7), at which point we will need to re-examine the full planing system to capture the further motion of the planing body.

5. Conclusion

The skimming process of a smooth body on shallow water can be divided into two consecutive stages: an impact and a planing stage. During the impact stage in a short time-frame just after touchdown, the body's wetted leading and trailing separation points evolve according to the square root of time, their speed slows as time grows; on the vertical scale the body penetrates deeper into water until shortly before the end of the impact stage, at which point the fluid-body contact area grows sufficiently large and the hydrodynamic pressure begins to lift the body upwards. A region of

positive (adverse) pressure gradient starts to develop ahead of the trailing separation position towards the end of this stage; this area grows over time and eventually reaches the separation position, at which point the trailing spray jet disappears and the impact stage terminates. We find that a body with sufficiently small mass and a positive rotation is able to transition rapidly from the impact to the planing stage.

The value of the adverse pressure gradient at the trailing separation point plays a critical role during the planing stage, with a limit on the maximum sustainable adverse pressure gradient. It is notable that rationally determining the precise value of the adverse pressure gradient itself is difficult at present because the detailed process of flow separation here involving a water-air interface and boundary layer is still unknown. Exceeding this limit the trailing separation flow may become more complex and the present planing model breaks down. The body otherwise is able to sustain the planing motion, during which both its leading and trailing separation points move in the upstream direction for a body with positive rotation, and it has a positive vertical motion as in a process of lifting-off from the water.

Of particular interest is the case where this adverse pressure gradient is small, for which we find the body's planing motion can be further divided into three phases: in the first phase the trailing separation position goes through a rapid transition towards the upstream direction, which reduces the length of the body-fluid contact region to a scale that is proportional to the body's mass in a predetermined time-frame; in the second phase the leading and trailing separation points move in the direction of upstream linearly with time as the body rotates forwards, and its vertical position evolves rapidly to the cubic power of time and grows out of this regime in a short period of time; in the final planing phase the two separation points continue to evolve linearly with time, while the body's vertical position moves upwards according to the squared power of time. Under this rapidly planing regime although we do not witness the phenomenon of the planing body lifting-off from the water thus far, it is clear that a slightly larger time scale should capture that phenomenon.

References

[1] Korobkin A. A. and Scolan Y. M. Three-dimensional theory of water impact. Part 2. Linearized Wagner problem. *J. Fluid Mech.*, 549, 2006.

[2] Green A. E. The gliding of a plate on a stream of finite depth. *Proc. Camb. Phil. Soc.*, 31, 1935.

[3] Green A. E. The gliding of a plate on a stream of finite depth. Part II. *Proc. Camb. Phil. Soc.*, 32, 1936.

[4] Batyaev E. A. and Khabakhpasheva T. I. Initial stage of the inclined impact of a smooth body on a thin fluid layer. *Fluid Dynamics*, 48(2), 2013.

[5] Tuck E. O. and Dixon A. Surf-skimmer planing hydrodynamics. *J. Fluid Mech.*, 205, 1989.

[6] K. Beswick et al. Properties of small cirrus ice crystals from commercial aircraft measurements and implications for flight operations. *Tellus B: Chemical and Physical Meteorology*, 68(27876), 2016.

[7] Streckwall H., Lindenau O., and Bensch L. Aircraft ditching: a free surface/free motion problem. *Archives of civil and mechanical engineering*, VII(3), 2007.

[8] Wagner H. Landing of seaplanes. *NACA*, TM(622), 1931.

[9] Wagner H. Über Stoß-und gleitvorgänge an der Oberflaäche von Flüssigkeiten (Phenomena associated with impacts and sliding on liquid surfaces). *Zeitschr. Math. Mech.*, 12, 1932.

[10] Watanabe I. Analytical expression of hydrodynamic impact pressure by matched asymptotic expansion technique. *Trans. West-Japan Soc. Naval Arch.*, 71, 1986.

[11] Hewitt I. J., Balmforth N. J., and McElwaine J. N. Continual skipping on water. *J. Fluid Mech.*, 2011.

[12] Oliver J. M. Water entry and related problems. *PhD Thesis*, 2002.

[13] Liu K. and Smith F. T. Collisions, rebounds and skimming. *Phil Trans Roy Soc A*, 372, 2014.

[14] Jia Liu. *Shallow water skimming, skipping and rebound problems.* PhD thesis, UCL, 2017.

[15] Greenhow M. Water-entry and -exit of a horizontal circular cylinder. *Appl. Ocean Res.*, 10(4), 1988.

[16] Reinhard M., Korobkin A. A., and Cooker M. J. The bounce of a blunt body from a water surface at high horizontal speed. *27th International Workshop on Water Waves and Floating Bodies*, 2012.

[17] Faltinsen O. M., Landrini M., and Greco M. Slamming in marine applications. *J. Engng Maths*, 48, 2004.

[18] U.S. Department of Transportation Federal Aviation Administration. *Seaplane, skiplane and float/ski equipped helicopter operations handbook FAA-H-8083-23.* 2004.

[19] Hicks P. D. and Smith F. T. Skimming impacts and rebounds on shallow liquid layers. *Proc. R. Soc.*, 2010.

[20] Cointe R. and Armand J. L. Hydrodynamic impact analysis of a cylinder. *ASME J. Offshore Mech. Arc. Engng*, 109, 1987.

[21] Palmer R. and Smith F. T. Skimming impacts and rebounds of smoothly shaped bodies on shallow liquid layers. *J. Engng, Math.*, 2020.

[22] Edge R. D. The surf skimmer. *Am. J. Phys*, 36, 1968.

[23] Howison S. D., Ockendon J. R., and Oliver J. M. Oblique slamming, planing and skimming. *J. Engng Math.*, 48, 2004.

[24] Howison S. D., Ockendon J. R., and Wilson S. K. Incompressible water-entry problems at small deadrise angles. *J. Fluid Mech.*, 222, 1991.

[25] Von Kármán T. The impact of seaplanes floats during landing. *NACA*, TN(321), 1929.

[26] Khabakhpasheva T. I. and Korobkin A. A. Oblique impact of a smooth body on a thin layer of liquid. *Proc. R. Soc.*, (469), 2013.